THE JOURNAL OF PHYSICAL CHEMISTRY Letters

Letter

pubs.acs.org/JPCL

Conditional Born–Oppenheimer Dynamics: Quantum Dynamics Simulations for the Model Porphine

Guillermo Albareda,*[,†,‡] Josep Maria Bofill,[†,§] Ivano Tavernelli,[∥] Fermin Huarte-Larrañaga,[†,‡] Francesc Illas,[†,‡] and Angel Rubio*[,⊥,¶,▽]

[†]Institut de Química Teòrica i Computacional, Universitat de Barcelona, Barcelona 08028, Spain

[‡]Departament de Química Física, Universitat de Barcelona, Barcelona 08028, Spain

[§]Departament de Química Orgànica, Universitat de Barcelona, Barcelona 08028, Spain

[∥]IBM Research Zurich, Säumerstrasse 4, 8803 Rüschlikon, Switzerland

[⊥]Max Planck Institute for the Structure and Dynamics of Matter, Luruper Chaussee 149, 22761 Hamburg, Germany

[¶]Center for Free-Electron Laser Science & Department of Physics, University of Hamburg, Luruper Chaussee 149, 22761 Hamburg, Germany

[▽]Nano-Bio Spectroscopy Group and ETSF, Departamento Fisica de Materiales, Universidad del País Vasco, CFM CSIC-UPV/EHU-MPC & DIPC, 20018 San Sebastián, Spain

ABSTRACT: We report a new theoretical approach to solve adiabatic quantum molecular dynamics halfway between wave function and trajectory-based methods. The evolution of a *N*-body nuclear wave function moving on a 3*N*-dimensional Born–Oppenheimer potential-energy hyper-surface is rewritten in terms of single-nuclei wave functions evolving nonunitarily on a 3-dimensional potential-energy surface that depends parametrically on the configuration of an ensemble of generally defined trajectories. The scheme is exact and, together with the use of trajectory-based statistical techniques, can be exploited to circumvent the calculation and storage of many-body quantities (e.g., wave function and potential-energy surface) whose size scales exponentially with the number of nuclear degrees of freedom. As a proof of concept, we present numerical simulations of a 2-dimensional model porphine where switching from concerted to sequential double proton transfer (and back) is induced quantum mechanically.

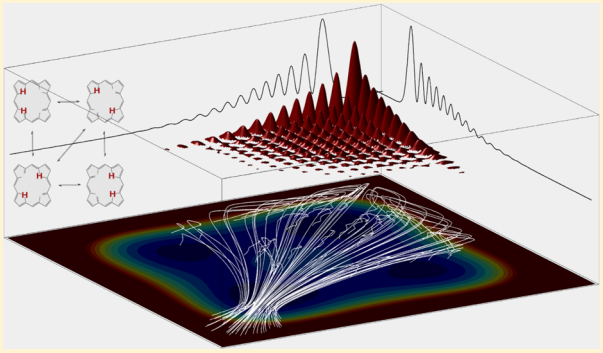

On the basis of the Born–Huang expansion of the molecular wave function,[1] an exact description of adiabatic molecular dynamics requires the propagation of a nuclear wavepacket on the ground-state Born–Oppenheimer potential-energy surface (gs-BOPES). This propagation scheme is, somehow, computationally doubly prohibitive. Besides the computational burden associated with the propagation of the (many-body) nuclear wave function, the calculation of the gs-BOPES constitutes, per se, a time-independent problem that grows exponentially with the number of electrons and nuclei. In this respect, two main classes of computational methods have emerged depending on whether the knowledge of the gs-BOPES is required in the full configuration space, that is, full-quantum methods,[2,3] or only at certain reduced number of points, namely trajectory-based or direct methods.[4,5] While methods for computing the energy of any configuration of nuclei have become quicker and more accurate, full-quantum dynamics calculations still become rapidly unfeasible for large molecules. Alternatively, direct dynamics notably reduce the computational cost of the simulations by avoiding partially, sometimes completely, the calculation of the full gs-BOPES (this can be done, for instance, by the use of reaction-path Hamiltonians[6,7]). Nuclear quantum effects, however, can be hardly included systematically in this second class of methods. Up to date, only quantum-trajectory methods have the particularity of being able to describe all nuclear quantum effects (just as full-quantum methods) and being on-the-fly simultaneously.[8−11] Unfortunately, these methods have serious problems in dealing with the so-called quantum potential, which gathers, by definition, all quantum information on the system. The mathematical structure of the quantum potential depends on the inverse of the quantum probability density, and thus, its manipulation entails serious instability problems.[12−14]

We report here an exact theoretical approach to solve adiabatic quantum molecular dynamics based on the use of conditional wave functions (CWFs), halfway between full-quantum and trajectory-based methods. Whereas the concept of CWF is owing to the formulation of the quantum

Received: February 27, 2015
Accepted: April 2, 2015
Published: April 2, 2015

DOI: 10.1021/acs.jpclett.5b00422
J. Phys. Chem. Lett. 2015, 6, 1529−1535

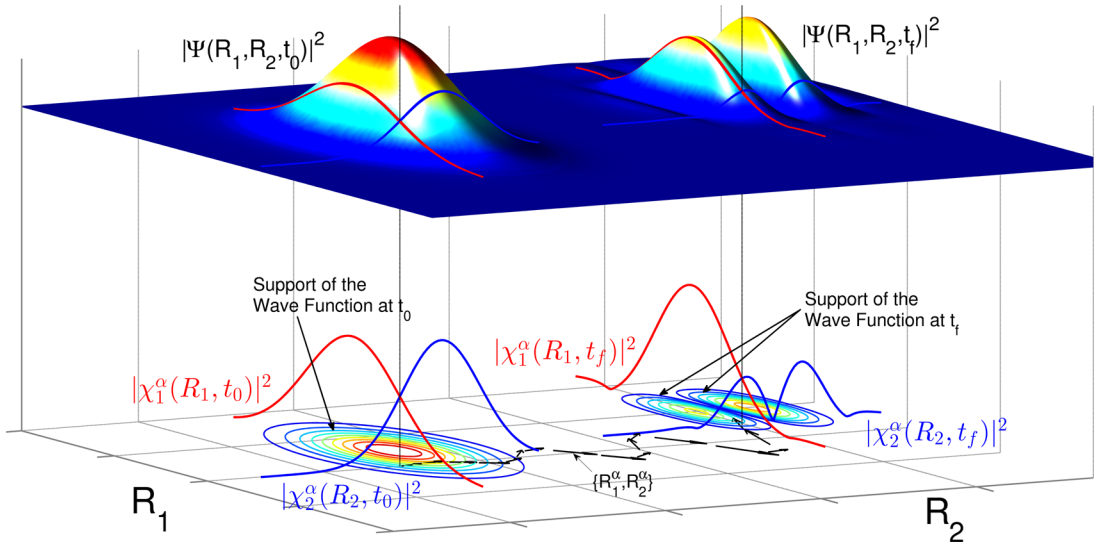

Figure 1. Schematic representation of the conditional wave function for a simple 2-dimensional scenario. The full nuclear probability-density $|\Psi(R_1, R_2, t)|^2$ is plot at two different times t_0 and t_f, together with the conditional probability densities $|\chi_1^\alpha(R_1,t)|^2$ (in red) and $|\chi_2^\alpha(R_2, t)|^2$ (in blue) for a particular trajectory $\{R_1^\alpha(t), R_2^\alpha(t)\}$. Black arrows for the velocity field $\{v_1^\alpha(t), v_2^\alpha(t)\}$, and contour plots of the full nuclear wave function are also shown for clarity.

measurement problem in Bohmian mechanics,[13,15] it can still be applied to general bipartite quantum systems. The wave function associated with N degrees of freedom can be exactly rewritten in terms of an ensemble of CWFs associated with a subgroup of $M(<N)$ degrees of freedom. The corresponding equations of motion are nonunitary and depend parametrically on trajectories that, ideally, span the full support of the probability density in the configuration space. This idea has been successfully applied to split-up the many-body electronic wave function in quantum transport problems[16−20] and also to rewrite the equations of motion of electrons and nuclei for nonadiabatic molecular dynamics without the use of BOPESs.[21] We focus here on the adiabatic evolution of N nuclei on the corresponding gs-BOPES and demonstrate that a conditional decomposition of its many-body wave function leads to a new class of "quasidirect" molecular dynamics methods.

Throughout this Letter, we use atomic units, and nuclear coordinates are collectively denoted by $\mathbf{R} = \{\mathbf{R}_1, ..., \mathbf{R}_N\}$. In the Born−Oppenheimer limit, the Born−Huang expansion[1] of the molecular wave function provides a Schrödinger-like equation of motion for the nuclear wave function $\Psi(\mathbf{R}, t)$

$$i\partial_t\Psi(\mathbf{R}, t) = \Big(\sum_{k=1}^{N}\hat{T}_k + \epsilon(\mathbf{R})\Big)\Psi(\mathbf{R}, t) \tag{1}$$

where $\hat{T}_k = -\nabla_k^2/(2M_k)$ is the kinetic energy operator of the kth nuclei. The scalar potential $\epsilon(\mathbf{R})$ is the $3N$-dimensional gs-BOPES defined through $\hat{H}_e\Phi_{\mathbf{R}}(\mathbf{r}) = \epsilon(\mathbf{R})\Phi_{\mathbf{R}}(\mathbf{r})$, with $\hat{H}_e(\mathbf{r},\mathbf{R})$ being the standard electronic Hamiltonian and $\mathbf{r}$ collecting all electronic coordinates. The nuclear wave function $\Psi(\mathbf{R}, t)$ in eq 1 can be exactly decomposed in terms of an ensemble of single-nuclei CWFs, labeled α, defined as

$$\chi_k^\alpha(\mathbf{R}_k, t) := \Psi(\mathbf{R}, t)|_{\bar{\mathbf{R}}_k^\alpha(t)} \tag{2}$$

where $\bar{\mathbf{R}}_k = \{\mathbf{R}_1, ..., \mathbf{R}_{k-1}, \mathbf{R}_{k+1}, ..., \mathbf{R}_N\}$, and the ensemble of trajectories $\{\bar{\mathbf{R}}_k^\alpha(t)\}$ explores the support of $|\Psi(\mathbf{R}, t)|^2$ at any time t. To see that, we only need to realize that the CWFs can be used to reconstruct the full nuclear wave function as $\Psi(\mathbf{R}, t) = \hat{\mathcal{D}}_{\bar{\mathbf{R}}_k}[\chi_k^\alpha(\mathbf{R}_k,t)]$, where the transformation $\hat{\mathcal{D}}_{\bar{\mathbf{R}}_k}[f(\bar{\mathbf{R}}_k^\alpha)] = [\sum_{\alpha=1}^{\infty}\delta(\bar{\mathbf{R}}_k^\alpha - \bar{\mathbf{R}}_k)f(\bar{\mathbf{R}}_k^\alpha)]/[\sum_{\alpha=1}^{\infty}\delta(\bar{\mathbf{R}}_k^\alpha - \bar{\mathbf{R}}_k)]$ connects the (parametrized) single-nuclear subspace with the full configuration space.[21] Notice that in order to avoid singularities due to the formation of nodes, the following condition is also required: $\Psi(\mathbf{R}, t) = 0$, whenever $\sum_{\alpha=1}^{\infty}\delta(\bar{\mathbf{R}}_k^\alpha - \bar{\mathbf{R}}_k) = 0$.

For simplicity, we omit from now on the explicit time-dependence of the trajectories, that is, $\mathbf{R}^\alpha = \{\mathbf{R}_1^\alpha(t), ..., \mathbf{R}_N^\alpha(t)\}$, in particular $\bar{\mathbf{R}}_k^\alpha = \bar{\mathbf{R}}_k^\alpha(t)$. By evaluating eq 1 at $\bar{\mathbf{R}}_k^\alpha$, equations of motion for each CWF, $\chi_k^\alpha(\mathbf{R}_k,t)$, are immediately found

$$\begin{aligned} i\partial_t\chi_k^\alpha(\mathbf{R}_k, t) = &(\hat{T}_k + \epsilon^\alpha(\mathbf{R}_k))\chi_k^\alpha(\mathbf{R}_k, t) \\ &+ \sum_{j\neq k}^{N}\hat{T}_j\Psi(\mathbf{R}, t)|_{\bar{\mathbf{R}}_k^\alpha} + i\sum_{j\neq k}^{N}\nabla_j\Psi(\mathbf{R}, t)|_{\bar{\mathbf{R}}_k^\alpha}\cdot\dot{\mathbf{R}}_j^\alpha \end{aligned} \tag{3}$$

The conditional gs-BOPES, $\epsilon^\alpha(\mathbf{R}_k)$, entering eq 3 is now a single-nuclei quantity defined through

$$\hat{H}_e^\alpha\Phi_{\bar{\mathbf{R}}_k^\alpha}(\mathbf{R}_k, \mathbf{r}) = \epsilon^\alpha(\mathbf{R}_k)\Phi_{\bar{\mathbf{R}}_k^\alpha}(\mathbf{R}_k, \mathbf{r}) \tag{4}$$

where $\hat{H}_e^\alpha(\mathbf{r}, \mathbf{R}_k)$ is the electronic Hamiltonian evaluated at $\bar{\mathbf{R}}_k^\alpha$. Each CWF, $\chi_k^\alpha(\mathbf{R}_k, t)$, is thus a 3-dimensional slice of the full nuclear wave function taken along the kth coordinate (a schematic representation of the CWF can be found in Figure 1 for a simple 2-dimensional scenario). Each CWF constitutes an open quantum system: its evolution is nonunitary due to the last two terms in eq 3, in general complex functionals of the full wave function $\Psi(\mathbf{R}, t)$. In one hand, the last term in 3 is a pure advective term accounting for the fact that CWFs do move in configurational space guided by the trajectories $\bar{\mathbf{R}}_k^\alpha$ (schematically depicted in Figure 1). It can be simply defined as the difference between the total and the partial time derivative of the CWF, viz. $\sum_{j\neq k}^{N}\nabla_j\Psi|_{\bar{\mathbf{R}}_k^\alpha}\cdot\dot{\mathbf{R}}_j^\alpha = d_t\chi_k^\alpha - \partial_t\chi_k^\alpha$. On the other hand, the first complex potential in eq 3, $\sum_{j\neq k}^{N}\hat{T}_j\Psi|_{\bar{\mathbf{R}}_k^\alpha}$ is the kinetic correlation accounting for the interaction among CWFs. In most general conditions, both the advective and the kinetic correlation terms are necessary to preserve the norm of the full wave function and also the total energy of the nuclear system.[21]

DOI: 10.1021/acs.jpclett.5b00422
J. Phys. Chem. Lett. 2015, 6, 1529−1535

In order to propose a self-consistent propagation scheme based on eq 3, it still remains to define the trajectories $\{\mathbf{R}_k^\alpha\}$. The only requirement to be fulfilled by these trajectories is that they explore the support of the quantum probability density $\rho = |\Psi(\mathbf{R}, t)|^2$ (also shown in Figure 1). Notice that for the simplest case where $\dot{\mathbf{R}}_k^\alpha = 0$, there is no advection, and thus, eq 3 reduces to eq 1. Alternatively, other choices of $\{\mathbf{R}_k^\alpha\}$ can be used to circumvent the use of computationally demanding fixed-grid methods. Here we choose $\{\mathbf{R}_k^\alpha\}$ to be Bohmian trajectories because they do sample the quantum probability density and provide in addition an intuitive picture of quantum dynamics.[13,22−27] Specifically, because eq 1 is compatible with a local conservation of particles, $\partial_t \rho = \sum_{k=1}^{N} \nabla_k(\rho \mathbf{v}_k)$, we can interpret the quantum probability density, ρ, as the spatial distribution of an ensemble of trajectories with velocities defined through the phase of the many-body nuclear wave function, $\mathbf{v}_k(\mathbf{R}, t) = (\nabla_k S)/M_k$, where $\Psi(\mathbf{R}, t) = |\Psi(\mathbf{R}, t)| e^{iS(\mathbf{R}, t)}$. In practice, the reconstruction of the full nuclear phase $S(\mathbf{R}, t)$ can be avoided at the expense of solving N times the number of equations of motion.[16,17,21] In this way, quantum trajectories can be computed as

$$\mathbf{R}_k^\alpha(t) = \mathbf{R}_k^\alpha(t_0) + \int_{t_0}^{t} \mathbf{v}_k^\alpha(\mathbf{R}_k^\alpha(t'), t')\mathrm{d}t' \tag{5}$$

where $\mathbf{v}_k^\alpha(\mathbf{R}_k^\alpha, t) = (\nabla_k S_k^\alpha/M_k)|_{\mathbf{R}_k^\alpha} := \mathbf{v}_k(\mathbf{R}^\alpha, t)$ are called conditional velocity fields, and $S_k^\alpha(\mathbf{R}_k, t)$ are the phases of the nuclear CWFs $\chi_k^\alpha = |\chi_k^\alpha| e^{iS_k^\alpha}$.

In the remaining part of the Letter, we explore a first approximation to this general method to solve quantum adiabatic dynamics. We assume a zero order expansion of the complex functionals in eq 3 around each nuclear variable. More specifically, $\hat{T}_j \Psi|_{\bar{\mathbf{R}}_k^\alpha} + i(\nabla_j \Psi)|_{\bar{\mathbf{R}}_k^\alpha} \cdot \dot{\mathbf{R}}_j^\alpha = f_k(\bar{\mathbf{R}}_k^\alpha, t)$. Because this approximation corresponds to a Hermitian limit of eq 3, the time evolution of $\chi_k^\alpha(\mathbf{R}_k, t)$ becomes unitary. This means that the integration of the full Schrödinger equation is made now slice by slice. The approximated functionals entail now only pure time-dependent phases that can be omitted because the velocity fields, $\mathbf{v}_k^\alpha(\mathbf{R}_k t)$, are invariant under global phase transformations.[16,21] We call the resulting propagation scheme, that is, eq 5 together with the Hermitian limit of eq 3, *Hermitian adiabatic approach* (HAA). Remarkably, the HAA does not require the computation of the quantum potential, in this manner overcoming a bottleneck in quantum trajectory-based approaches.[12,28−31]

In order to demonstrate the accuracy of the HAA to describe quantum molecular dynamics, we chose the model porphine as designed by Smedarchina et al.[32] and later used by Accardi et al.[33] to describe the switch from synchronous (or concerted) to sequential (or stepwise) double-proton transfer. This model accounts for the motions of two protons (labeled 1 and 2) along coordinates R_1 and R_2, respectively, from the domains of the reactant (R) to the product (P) (see Figure 2). The PES model is[32]

$$V(R_1, R_2) = \frac{U_0}{\Delta_0^4}[(R_1^2 - \Delta_0^2)^2 + (R_2^2 - \Delta_0^2)^2 - 4G\Delta_0^2 R_1 R_2] + 2G(2 + G)U_0 \tag{6}$$

We choose here the same parameters used by Accardi et al.[33] The parameter $U_0 = 0.473$ eV has been fitted in ref 32. in order to account for the experimental results of nuclear magnetic resonance and laser-induced fluorescence measurements of refs

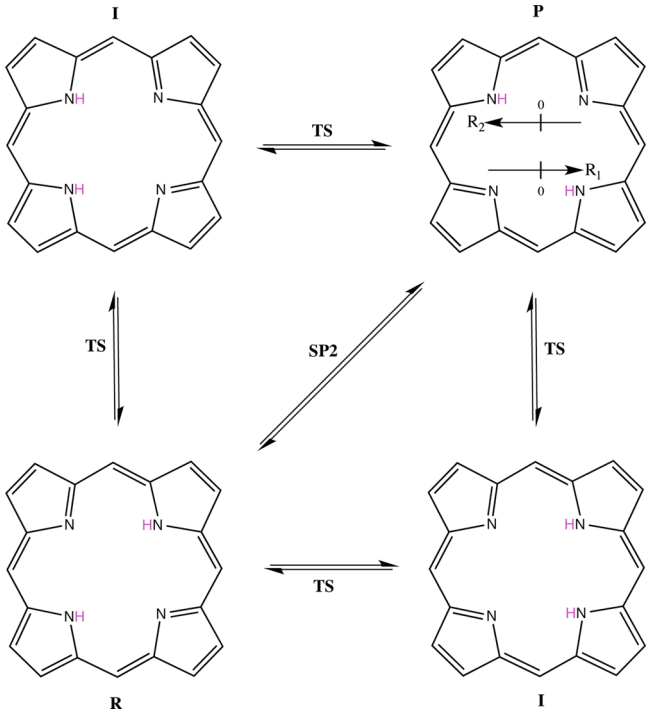

Figure 2. Double proton tranfer for the model porphine. The protons move along coordinates R_1 and R_2. The four snapshots represent the transfer of the two protons from reactant (R) to product (P), sequentially along intermediate states (I) involving four transition states (TS), or simultaneously through a second order saddle point (SP2).

34−36. The other two parameters, $\Delta_0 = 1.251a_0$ and $G = 0.063$ are based on density functional theory calculations of Smedarchina et al.[37] at the B3LYP/6-31G* level. The resulting 2D model PES is illustrated in Figure 3. The barriers are labeled TS ("transition states") for two alternative reaction paths. The reaction can lead from the reactant R via alternative transitions states TS to the intermediates (I), and subsequently via the

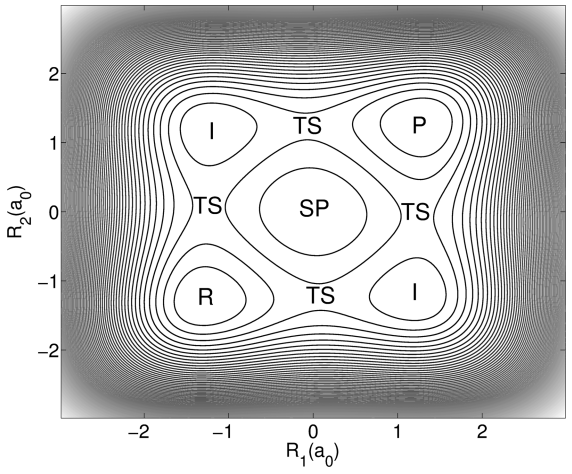

Figure 3. Potential energy surface for the model porphine, eq 6, adopted from refs 32 and 33. The equidistant values of the contours range from 0 eV, for the potential minima for the reactant (R) and product (P) configurations, to 2 eV. The corresponding energies of the local minima for the intermediates (I), of the four barriers labeled TS, and of the second order saddle point (SP2) are 0.238, 0.600, and 1.069 eV, respectively.

DOI: 10.1021/acs.jpclett.5b00422
J. Phys. Chem. Lett. 2015, 6, 1529−1535

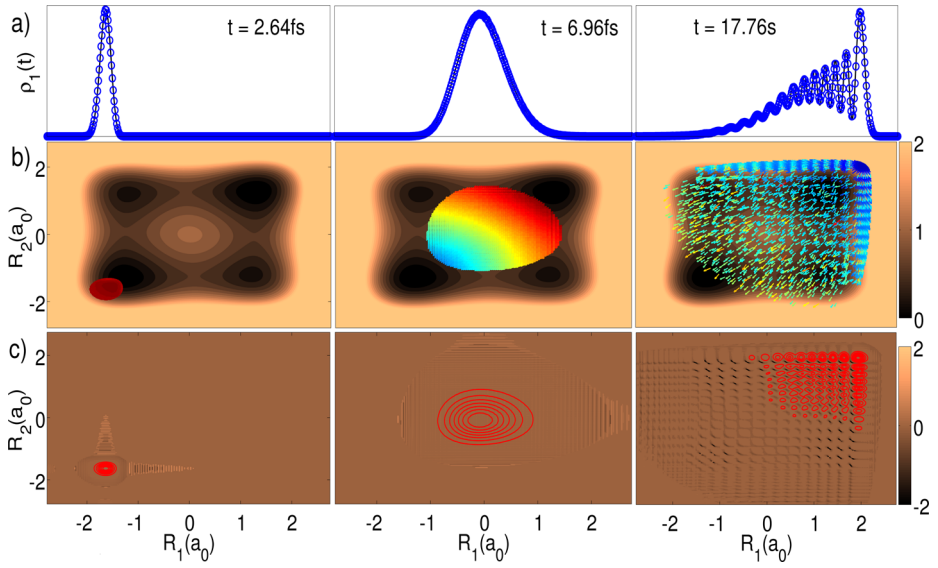

Figure 4. Snapshots of the nuclear dynamics for the model porphine from t = 2.64 fs to t = 17.76 fs. (a) reduced probability density in arbitrary units for the exact solution in black solid-line and for the approximated solution, using CWFs, in blue circles. The density has been renormalized as $\rho_1(R_1, t)/\max(\rho_1(R_1, t))$. (b) Colored arrows, from dark blue (minimum velocity) to dark red (maximum velocity), represent the velocity field, $\{v_1(R_1, R_2, t), v_2(R_1, R_2, t)\}$, imposed over contour-plots of the gs-BOPES that range from 0 to 2 eV. (c) Contour-plot of the full probability density (in red) on top of the quantum potential (limited from −2 eV to 2 eV). The exact solution of eq 1 was obtained using a fourth-order Runge−Kutta integration scheme together with a sixth-order finite differences representation of the system Hamiltonian on a regular square grid. The HAA propagation scheme was identically integrated within a 1-dimensional equidistant grid. Time and spatial steps of Δt = 0.1 au and $\Delta R_1 = \Delta R_2 = 0.017a_0$ where used in both cases.

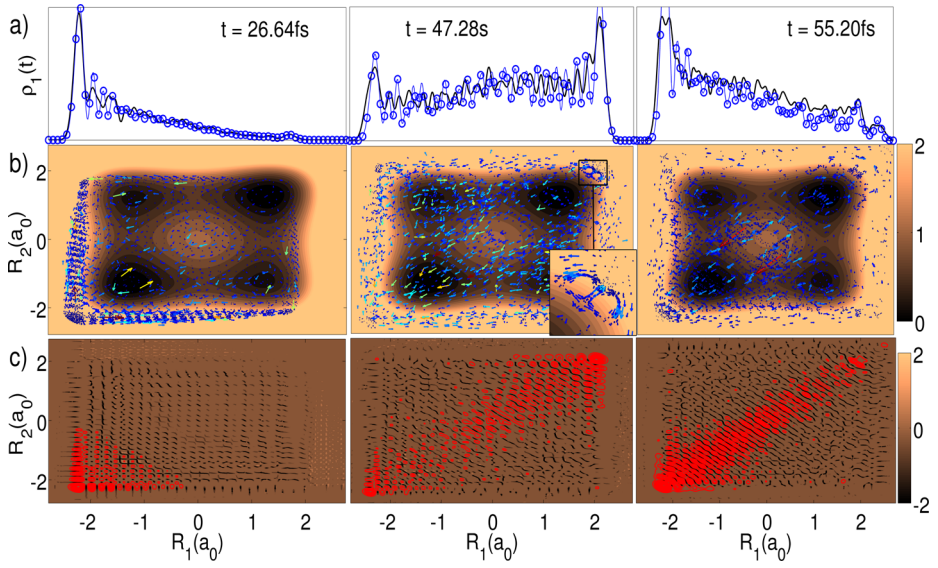

Figure 5. Snapshots of the nuclear dynamics for the model porphine starting from t = 26.64 fs to t = 55.20 fs. (a) reduced probability density in arbitrary units for the exact solution in black solid-line and for the approximated solution, using CWFs, in blue circles. The density has been renormalized as $\rho_1(R_1, t)/\max(\rho_1(R_1, t))$. (b) Colored arrows, from dark blue (minimum velocity) to dark red (maximum velocity), represent the velocity field, $\{v_1(R_1, R_2, t), v_2(R_1, R_2, t)\}$, imposed over contour-plots of the gs-BOPES that range from 0 to 2 eV. (c) Contour-plot of the full probability density (in red) on top of the quantum potential (limited from −2 eV to 2 eV). The exact solution of eq 1 was obtained using a fourth-order Runge−Kutta integration scheme together with a sixth-order finite differences representation of the system Hamiltonian on a regular square grid. The HAA propagation scheme was identically integrated within a 1-dimensional equidistant grid. Time and spatial steps of Δt = 0.1au and $\Delta R_1 = \Delta R_2 = 0.017a_0$ where used in both cases.

other two TS to the product P. In addition, Figure 3 shows a central saddle point (of second order) labeled SP2. The competing synchronous reaction mechanism leads from the reactant R via SP2 to the product P (see Figure 2). The model potential, eq 6, is symmetric with respect to the diagonals $R_1 = \pm R_2$. It accommodates nearly degenerate doublets of eigenstates $\Psi_{v+}(R_1, R_2)$ and $\Psi_{v-}(R_1, R_2)$, with energies below the barriers TS, plus higher excited states. Following Accardi et al.,[33] to define the initial state $\Psi(R_1, R_2, t = 0)$, we determine, first of all, the wave functions $\Psi_{0+}(R_1, R_2)$ and $\Psi_{0-}(R_1, R_2)$ of the lowest doublet ($v = 0$). We then chose our initial state to be $\Psi(R_1, R_2, t = 0) = \Psi_{0,R}(R_1 + \Delta R, R_2 + \Delta R)$ with $\Delta R = -1a_0$, where $\Psi_{0,R}(R_1,R_2) = (1/\sqrt{2})(\Psi_{0+} + \Psi_{0-})$ is a superposition state that represents the localized ground state wave function of

DOI: 10.1021/acs.jpclett.5b00422
J. Phys. Chem. Lett. 2015, 6, 1529−1535

the reactant (the details on how this initial state can be experimentally achieved can be read in ref 33). The mean energy of the initial state is 4.885 eV, well above the values of the barriers TS (0.600 eV), and also the saddle point SP2, (1.069 eV), so we do not expect remarkable tunneling effects during the first forward reaction.

Starting with $\Psi(R_1, R_2, t = 0)$, we first sample its probability density with trajectories[13,38] and then propagate eq 5 together with the Hermitian limit of eq 3. Figures 4a and 5a show snapshots at different times of the one-particle reduced nuclear probability density, computed as $\rho_1(R_1, t) = \int dR_2 |\Psi(R_1, R_2, t)|^2$ from the solution of eq 1 (in black solid line), and computed as $\rho_1(R_1, t) = \int dR_2\ \hat{\mathcal{D}}_{R_2}[|\chi_1^\alpha(R_1, t)|^2]$ for the approximated solution (in blue circles). We gain insight into this reaction by analyzing the quantum velocity fields $v_1^\alpha(R_1, t)$ and $v_2^\alpha(R_2, t)$ computed from the approximated conditional wave functions $\chi_1^\alpha(R_1, t)$ and $\chi_2^\alpha(R_2, t)$ respectively. Snapshots of these velocity fields in terms of colored arrow maps are displayed in Figures 4b and 5b together with the 2-dimensional gs-BOPES. The importance of quantum effects in the nuclear dynamics is revealed in Figures 4c and 5c, where we superimpose contour plots of the full probability density (in red) over the quantum potential, computed from the exact solution as $Q(R_1, R_2, t) = (-1/(2M))[(\nabla_{R_1}^2\sqrt{\rho})/\sqrt{\rho} + (\nabla_{R_2}^2\sqrt{\rho})/\sqrt{\rho}]$.[13,38,39]

The initial synchronous mechanism of the first forward reaction is characterized by an initial squeezing followed by rapid dispersion of the wavepacket. At time t = 2.64 fs, the wavepacket (initially designed to seat at the minimum of the gs-BOPES) is squeezed due to its progressive accommodation to the reactant valley. As shown in Figure 4c, a non-negligible quantum contribution to the squeezing comes from the formation of quantum potential walls that compress the wavepacket during its propagation. The switch from the synchronous to sequential mechanism is mediated by two distinct effects: first, the wavepacket dispersion (at time t = 6.96 fs), and second, relief reflections of the broadened wavepacket from wide regions of the steep repulsive wall of the PES close to the minimum of the product (at time t = 17.76 fs). The density as well as the velocity field discover relief reflections[40] of different parts of the wave function into different directions. Figure 4c at time t = 17.76 fs, shows three major directions of the scattered waves, one of them returning back toward the direction of SP2, the other two equivalent partial waves pointing toward the two intermediates states I. The quantum potential shows a well-defined grid structure with minima surrounding each unit cell (at t = 17.76 fs). This pattern of the quantum potential can be understood as the ultimate responsible of the rising of relief interferences and the switch from concerted to mixed double proton transfer. The consecutive minima of the quantum potential induces a well-defined pattern of fringes in Figure 4b corresponding to alternate fast (light blue) and slow (dark blue) nuclear velocities. This is directly translated into the formation of relief interferences (see Figure 4a,c at t = 17.76 fs). This situation is reminiscent of the near field interference effect arising when periodic diffracting structures are illuminated by highly coherent light or particle beams[41] (the three partial waves pointing to I and SP2 play here the role of a diffracted wavepacket by three slits). Later on, at t = 26.64 fs, the probability density at the reactant achieves its second maximum (see Figure 5). Though most parts of the wave function are going back to the domain P of the product, there are still some other slower parts which are lack behind. The time dilatation supported by continuous wavepacket dispersion leads to a strong proton delocalization (at time t = 47.28 fs). The interference patterns become more and more fuzzy during the second forward reaction. This is translated into a complicate velocity field distribution that gives rise to complex phenomena such as quantum vortices (see the inset in Figure 5b at time t = 47.28 fs). This apparently "chaotic" flux is however fully coherent and ultimately directs the recovery of the concerted double proton transfer at t = 55.20 fs. Due to the strong time dilatation between partial waves, the grid structure of the quantum potential associated with the sequential double proton transfer progressively dilutes into what reminds a stationary state, showing a series of minima disposed perpendicular to the diagonal $R_1 = R_2$. Figure 5c at times t = 47.28 fs and t = 55.20 fs exemplifies this reverse switching from sequential to synchronous double proton transfer.

The above example demonstrates that the CWF method (even in its simplest hermitian form) is able to capture complex quantum dynamics on gs-BOPESs by preserving quantum coherence at relative long times. The HAA reproduces not only the conspicuous synchronous double proton transfer for the first forward reaction but also the interferences originating at later times that lead to subsequent mixed sequential-concerted reactions. Finally, notice that nuclear dynamics are, for this particular model problem, highly roaming. Due to the topology of the PES and the characteristics of the initial state, the 2D nuclear probability density rapidly spreads all over the surface. The exact nuclear trajectories are thus identically scattered all around. In this respect, it is worth mentioning that in our approach we are essentially solving the time-dependent molecular Schrödinger equation as a system of coupled, but fundamentally simpler (single-particle) equations of motion. Therefore, even for roaming dynamics, where the scaling of the number of required points of the gs-BOPES is not specially favorable, our method still has the advantage of dealing with single-particle wave functions.

To summarize, we present an exact decomposition of the (adiabatic) nuclear wave function in terms of single-nuclei CWFs defined in eq 2. Their evolution according to eq 3 does only require the manipulation of single-particle quantities such as the conditional gs-BOPESs in eq 4 or the CWF itself. The resulting propagation scheme lends itself as a rigorous starting point for developing new algorithms based on a new class of "quasidirect" molecular dynamics. We thus expect it to be of particular interest in scenarios where the involved number of nuclear degrees of freedom is large and quantum effects both complex and conspicuous. Although other kinds of trajectory-based statistical techniques (e.g., Feynman paths, geodesics, etc.) can been also used to guide the CWFs, Bohmian trajectories add an interpretative value to the method and together with the Hermitian limit of eq 3 provide a numerically stable algorithm (named HAA). We expect the validity of the HAA to break down for systems where advection or kinetic correlations become important. The solution of the equations of motion in eq 3 will then require the use of nonstandard propagation methods. In any event, it is encouraging that even a very simplified approximation of the method is able to reproduce complex nuclear dynamics accurately. We envision the development of more efficient/scalable algorithms based, for instance, on the combination of our method with density-functional-based propagation schemes or quantum-mechanics/molecular-mechanics mixed algorithms.

DOI: 10.1021/acs.jpclett.5b00422
J. Phys. Chem. Lett. 2015, 6, 1529−1535

AUTHOR INFORMATION

Corresponding Authors

*E-mail: albareda@ub.edu.

*E-mail: angel.rubio@mpsd.mpg.de.

Notes

The authors declare no competing financial interest.

ACKNOWLEDGMENTS

This work has been supported by Spanish MINECO through research grants CTQ2011-22505, CTQ2012-30751, CTQ2013-41307, and FIS2013-46159-C3-1-P, by Generalitat de Catalunya grants 2014SGR97, 2014SGR-0139, 2014SGR25, and XRQTC, and by Grupos Consolidados UPV/EHU del Gobierno Vasco (IT578-13). G.A. acknowledges additional financial support from the Beatriu de Pinós Program through Project No. 2010BP-A00069, F.I. acknowledges additional financial support through the 2009 ICREA Academia Award for Excellence in University Research, and A.R. acknowledges additional financial support from the European Research Council Advanced Grant DYNamo (ERC-2010- AdG-267374), the European Community FP7 project CRONOS (Grant number 280879-2) and COST Actions CM1204 (XLIC) and MP1306 (EUSpec).

REFERENCES

(1) Born, M.; Huang, K. *Dynamical Theory of Crystal Lattices (International Series of Monographs on Physics)*; Oxford University Press: Oxford, U.K., 1954.

(2) Zhang, J. Z. H. *Theory and Application of Quantum Molecular Dynamics*; World Scientific: Singapore, 1999.

(3) Beck, M.; Jäckle, A.; Worth, G.; Meyer, H.-D. The Multiconfiguration Time-Dependent Hartree (MCTDH) Method: a Highly Efficient Algorithm for Propagating Wavepackets. *Phys. Rep.* **2000**, *324*, 1−105.

(4) Marx, D.; Hutter, J. *Ab Initio Molecular Dynamics: Basic Theory and Advanced Methods*; Cambridge University Press: Cambridge, U.K, 2009.

(5) Truhlar, D. G. In *The Reaction Path in Chemistry: Current Approaches and Perspectives*; Understanding Chemical Reactivity; Heidrich, D., Ed.; Springer: The Netherlands, 1995; Vol. *16*; pp 229−255.

(6) Miller, W. H.; Handy, N. C.; Adams, J. E. Reaction Path Hamiltonian for Polyatomic Molecules. *J. Chem. Phys.* **1980**, *72*, 99−112.

(7) González, J.; Giménez, X.; Bofill, J. M. A Restricted Quantum Reaction Path Hamiltonian: Theory, Discrete Variable Representation Propagation Algorithm, and Applications. *J. Chem. Phys.* **2009**, *131*, 054108−054124.

(8) Curchod, B. F. E.; Tavernelli, I.; Rothlisberger, U. Trajectory-Based Solution of the Nonadiabatic Quantum Dynamics Equations: an O-the-Fly Approach for Molecular Dynamics Simulations. *Phys. Chem. Chem. Phys.* **2011**, *13*, 3231−3236.

(9) Curchod, B. F.; Tavernelli, I. On Trajectory-Based Nonadiabatic Dynamics: Bohmian Dynamics versus Trajectory Surface Hopping. *J. Chem. Phys.* **2013**, *138*, 184112−184130.

(10) Zamstein, N.; Tannor, D. J. Non-Adiabatic Molecular Dynamics with Complex Quantum Trajectories. I. The Diabatic Representation. *J. Chem. Phys.* **2012**, *137*, 22A517−22A523.

(11) Zamstein, N.; Tannor, D. J. Non-Adiabatic Molecular Dynamics with Complex Quantum Trajectories. II. The Adiabatic Representation. *J. Chem. Phys.* **2012**, *137*, 22A518−22A524.

(12) Tavernelli, I. Ab-Initio Driven Trajectory-Based Nuclear Quantum Dynamics in Phase Space. *Phys. Rev. A* **2013**, *87*, 042501−042513.

(13) Benseny, A.; Albareda, G.; Sanz, Á. S.; Mompart, J.; Oriols, X. Applied Bohmian Mechanics. *Euro. Phys. J. D* **2014**, *68*, 1−42.

(14) Garashchuk, S.; Rassolov, V.; Prezhdo, O. Semiclassical Bohmian Dynamics. *Rev. Comp. Chem.* **2011**, *27*, 287−335.

(15) Dürr, D.; Goldstein, S.; Zanghi, N. Quantum Equilibrium and the Origin of Absolute Uncertainty. *J. Stat. Phys.* **1992**, *67*, 843−907.

(16) Oriols, X. Quantum-Trajectory Approach to Time-Dependent Transport in Mesoscopic Systems with Electron-Electron Interactions. *Phys. Rev. Lett.* **2007**, *98*, 066803−066807.

(17) Albareda, G.; Suñé, J.; Oriols, X. Many-Particle Hamiltonian for Open Systems with Full Coulomb Interaction: Application to Classical and Quantum Time-Dependent Simulations of Nanoscale Electron Devices. *Phys. Rev. B* **2009**, *79*, 075315−075331.

(18) Albareda, G.; Marian, D.; Benali, A.; Yaro, S.; Zangh, N.; Oriols, X. Time-Resolved Electron Transport with Quantum Trajectories. *J. Comp. Electr.* **2013**, *12*, 405−419.

(19) Albareda, G.; Traversa, F. L.; Benali, A.; Oriols, X. Computation of Quantum Electrical Currents through the Ramo−Shockley−Pellegrini Theorem with Trajectories. *Fluctuation Noise Lett.* **2012**, *11*, 1242008−1242019.

(20) Benali, A.; Traversa, F. L.; Albareda, G.; Alarcón, A.; Agouthane, M.; Oriols, X. Effect of Gate-All-around Transistor Geometry on the High-Frequency Noise: Analytical Discussion. *Fluctuation Noise Lett.* **2012**, *11*, 1241002−1241013.

(21) Albareda, G.; Appel, H.; Franco, I.; Abedi, A.; Rubio, A. Correlated Electron-Nuclear Dynamics with Conditional Wave Functions. *Phys. Rev. Lett.* **2014**, *113*, 083003−083008.

(22) Sanz, Á. S., Miret-Artés, S. Lecture Notes in Physics *A Trajectory Description of Quantum Processes II. Applications*. Springer-Verlag: Heidelberg, Germany, 2014; Vol. *831*.

(23) Wyatt, R. E. *Quantum Dynamics with Trajectories: Introduction to Quantum Hydrodynamics*; Springer-Verlag: New York, U.S.A, 2006.

(24) Benseny, A.; Bagudà, J.; Oriols, X.; Mompart, J. Need for Relativistic Corrections in the Analysis of Spatial Adiabatic Passage of Matter Waves. *Phys. Rev. A* **2012**, *85*, 053619−053624.

(25) Wu, J.; Augstein, B. B.; Figueira de Morisson Faria, C. Local Dynamics in High-Order-Harmonic Generation Using Bohmian Trajectories. *Phys. Rev. A* **2013**, *88*, 023415−023422.

(26) Song, Y.; Li, S.-Y.; Liu, X.-S.; Guo, F.-M.; Yang, Y.-J. Investigation of Atomic Radiative Recombination Processes by the Bohmian-Mechanics Method. *Phys. Rev. A* **2013**, *88*, 053419−053426.

(27) Takemoto, N.; Becker, A. Visualization and Interpretation of Attosecond Electron Dynamics in Laser-Driven Hydrogen Molecular Ion Using Bohmian Trajectories. *J. Chem. Phys.* **2011**, *134*, 074309−074316.

(28) Lopreore, C. L.; Wyatt, R. E. Electronic Transitions with Quantum Trajectories. II. *J. Chem. Phys.* **2002**, *116*, 1228−1238.

(29) Gindensperger, E.; Meier, C.; Beswick, J. A. Mixing Quantum and Classical Dynamics Using Bohmian Trajectories. *J. Chem. Phys.* **2000**, *113*, 9369−9372.

(30) Prezhdo, O. V.; Brooksby, C. Quantum Backreaction through the Bohmian Particle. *Phys. Rev. Lett.* **2001**, *86*, 3215−3219.

(31) Additional discussions and analysis of relations of the presented HAA method with other, especially trajectory-based, algorithms such as Bohmian dynamics as approximated by Sophya Garashchuk,[42] complex trajectories as formulated by David Tannor,[11] entangled trajectories by Craig Martens[43] or quantized Hamiltonian dynamics by Oleg Prezhdo[44] would provide precious insights into the conditional wave function approach. Though we have already some preliminary results in this direction, findings are not yet conclusive. We are nonetheless committed to further elaborate on this important point.

(32) Smedarchina, Z.; Siebrand, W.; Fernández-Ramos, A. Correlated Double-Proton Transfer. I. Theory. *J. Chem. Phys.* **2007**, *127*, 174513−174526.

(33) Accardi, A.; Barth, I.; Kuhn, O.; Manz, J. From Synchronous to Sequential Double Proton Transfer: Quantum Dynamics Simulations for the Model Porphine. *J. Phys. Chem. A* **2010**, *114*, 11252−11262.

(34) Butenhoff, T. J.; Moore, C. B. Hydrogen Atom Tunneling in the Thermal Tautomerism of Porphine Imbedded in a *n*-Hexane Matrix. *J. Am. Chem. Soc.* **1988**, *110*, 8336−8341.

DOI: 10.1021/acs.jpclett.5b00422
J. Phys. Chem. Lett. 2015, 6, 1529−1535

(35) Braun, J.; Koecher, M.; Schlabach, M.; Wehrle, B.; Limbach, H.-H.; Vogel, E. NMR Study of the Tautomerism of Porphyrin Including the Kinetic HH/HD/DD Isotope Effects in the Liquid and the Solid State. *J. Am. Chem. Soc.* **1994**, *116*, 6593−6604.
(36) Braun, J.; Limbach, H.-H.; Williams, P. G.; Morimoto, H.; Wemmer, D. E. Observation of Kinetic Tritium Isotope Effects by Dynamic NMR. The Tautomerism of Porphyrin. *J. Am. Chem. Soc.* **1996**, *118*, 7231−7232.
(37) Smedarchina, Z.; Zgierski, M. Z.; Siebrand, W.; Kozlowski, P. M. Dynamics of Tautomerism in Porphine: an Instanton Approach. *J. Chem. Phys.* **1998**, *109*, 1014−1024.
(38) Oriols, X., Mompart, J. *Applied Bohmian Mechanics: From Nanoscale Systems to Cosmology*; Pan Stanford: Boca Raton, Florida, 2012.
(39) Holland, P. *The Quantum Theory of Motion: An Account of the De Broglie-Bohm Causal Interpretation of Quantum Mechanics*; Cambridge University Press: Cambridge, U.K., 1995.
(40) Gerber, R.; Korolkov, M. V.; Manz, J.; Niv, M. Y.; Schmidt, B. A Reflection Principle for the Control of Molecular Photodissociation in Solids: Model Simulation for F_2 in *Ar*. *Chem. Phys. Lett.* **2000**, *327*, 76−84.
(41) Sanz, Á. S.; Miret-Artés, S. A Causal Look into the Quantum Talbot Effect. *J. Chem. Phys.* **2007**, *126*, 234106−234117.
(42) Garashchuk, S.; Jakowski, J.; Wang, L.; Sumpter, B. G. Quantum Trajectory-Electronic Structure Approach for Exploring Nuclear Effects in the Dynamics of Nanomaterials. *J. Chem. Theor. Comp.* **2013**, *9*, 5221−5235.
(43) Donoso, A.; Martens, C. C. Quantum Tunneling Using Entangled Classical Trajectories. *Phys. Rev. Lett.* **2001**, *87*, 223202−223206.
(44) Prezhdo, O. V. Classical Mapping for Second-Order Quantized Hamiltonian Dynamics. *J. Chem. Phys.* **2002**, *117*, 2995−3002.

DOI: 10.1021/acs.jpclett.5b00422
J. Phys. Chem. Lett. 2015, 6, 1529−1535